Geophysical Journal International

*Geophys. J. Int.* (2014) **196,** 1770–1786
Advance Access publication 2013 December 24

doi: 10.1093/gji/ggt479

# Pseudo-dynamic source modelling with 1-point and 2-point statistics of earthquake source parameters

Seok Goo Song,[1] Luis A. Dalguer[1] and P. Martin Mai[2]

[1]*Swiss Seismological Service (SED), ETH Zurich, Zurich, Switzerland. E-mail: song@sed.ethz.ch*
[2]*Earth Science and Engineering, KAUST, Thuwal, Kingdom of Saudi Arabia*

Accepted 2013 November 22. Received 2013 October 21; in original form 2013 July 1

## SUMMARY

Ground motion prediction is an essential element in seismic hazard and risk analysis. Empirical ground motion prediction approaches have been widely used in the community, but efficient simulation-based ground motion prediction methods are needed to complement empirical approaches, especially in the regions with limited data constraints. Recently, dynamic rupture modelling has been successfully adopted in physics-based source and ground motion modelling, but it is still computationally demanding and many input parameters are not well constrained by observational data. Pseudo-dynamic source modelling keeps the form of kinematic modelling with its computational efficiency, but also tries to emulate the physics of source process. In this paper, we develop a statistical framework that governs the finite-fault rupture process with 1-point and 2-point statistics of source parameters in order to quantify the variability of finite source models for future scenario events. We test this method by extracting 1-point and 2-point statistics from dynamically derived source models and simulating a number of rupture scenarios, given target 1-point and 2-point statistics. We propose a new rupture model generator for stochastic source modelling with the covariance matrix constructed from target 2-point statistics, that is, auto- and cross-correlations. Our sensitivity analysis of near-source ground motions to 1-point and 2-point statistics of source parameters provides insights into relations between statistical rupture properties and ground motions. We observe that larger standard deviation and stronger correlation produce stronger peak ground motions in general. The proposed new source modelling approach will contribute to understanding the effect of earthquake source on near-source ground motion characteristics in a more quantitative and systematic way.

**Key words:** Earthquake dynamics; Earthquake ground motions; Computational seismology; Statistical seismology.



## 1 INTRODUCTION

Predicting ground motion characteristics for future earthquakes is an essential element in seismic hazard and risk analysis. Empirical prediction approaches have been widely used for these purposes because they are directly constrained by observed data (e.g. Abrahamson *et al*. 2008). However, their prediction capability is limited, especially in near-source regions for large events, where only limited data constraints are available. Simulation-based ground motion prediction approaches have become more popular due to a better understanding about earthquake source and wave propagation processes as well as increased high-performance computing capability. Physics-based computational approaches provide many interesting insights into finite source processes and their effects on near-source ground motion characteristics, which may also provide guidance in parametrizing empirical ground motion prediction models in a more physical manner.

Spontaneous dynamic rupture modelling has been successfully adopted in physics-based source and ground motion modelling for the last couple of decades (e.g. Andrews 1976; Day 1982; Olsen *et al*. 1997; Oglesby *et al*. 1998; Dalguer *et al*. 2008; Ripperger *et al*. 2008; Shi & Day 2013). The finite-faulting process in dynamic modelling is governed by first-order physical principles acting on the fault, such as stress and frictional behaviour. This physical basis enables us to generate physically self-consistent spatiotemporal evolution of finite source models. On the other hand, dynamic rupture modelling is computationally expensive, especially for large events that are typically embedded in a large computational domain. In addition, we may need to simulate a number of such rupture scenarios to cover a broad range of possible input parameters, which are generally poorly constrained by observations.

In this context, pseudo-dynamic source modelling has been introduced to retain the computational efficiency of kinematic source modelling, while simultaneously emulating source physics inferred

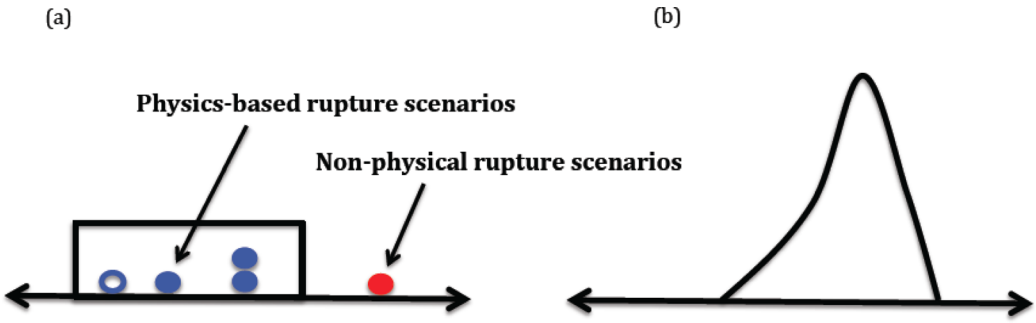


**Figure 1.** Quantifying the likelihood of rupture scenarios. (a) Non-zero, but uniform probability is assigned to physics-based (physically acceptable) rupture scenarios. Zero probability is assigned to non-physical rupture scenarios. (b) Non-uniform probability distribution within the physics-based rupture scenarios.

from rupture dynamics and observations (Guatteri *et al*. 2004; Liu *et al*. 2006; Schmedes *et al*. 2010; Song & Somerville 2010; Mena *et al*. 2012). However, it is still an open question how to construct an entirely self-consistent and statistically robust framework of the finite source process using the pseudo-dynamic approach. The key is to unravel in detail how exactly the rupture process determines ground motion characteristics, that is, how space–time correlations of kinematic source parameters affect near-field shaking and its spatial variability. In this paper, we extend and improve the concept of pseudo-dynamic source modelling, aiming for such a self-consistent statistical framework for physics-based source and ground motion modelling.

This study builds on previous work by Song & Somerville (2010), who propose a pseudo-dynamic source modelling method based on cross-correlation structures between kinematic source parameters, including both zero- and non-zero-offset correlations. Here, we extend their work as follows: (1) the concept of 1-point statistics (Song & Dalguer 2013) is included in both source characterization and modelling, (2) a new stochastic source modelling tool, based on the Cholesky factorization of a covariance matrix, is introduced in addition to the sequential Gaussian simulation with the kriging method (Song & Somerville 2010), (3) we compute ground motions using pseudo-dynamically generated source models, and quantitatively compare them with dynamically generated ground motions to investigate how statistical elements in the pseudo-dynamic source modelling influence ground motion characteristics.

## 2 SOURCE CHARACTERIZATION

### 2.1 Statistical framework for the finite source process

Given a target magnitude, many parameters are needed to characterize a finite-fault rupture model for ground motion simulation, such as rupture dimension (length and width), hypocentre location, heterogeneity of kinematic rupture parameters, etc. If we make the ergodic assumption, namely, that future events share finite source characteristics of past events, at least in a statistical sense, we may constrain some parameters for scenario events by studying past earthquakes. In classical kinematic source modelling, certain components of finite source models are simulated based on simple assumptions because they are not well constrained by data. In fact, this limitation applies to the temporal source parameters, such as rupture speed, slip velocity and slip duration, although these parameters play a significant role in determining near-source ground motion characteristics (Graves *et al*. 2008).

In this study, we extend pseudo-dynamic source modelling by formulating the finite source process in a statistical framework. The concept of pseudo-dynamic source modelling can be explained in a probabilistic sense, as illustrated in Fig. 1(a). We assign non-zero probability to physics-based rupture scenarios, and zero probability to non-physical rupture scenarios. By assigning zero probability to non-physical rupture scenarios, they are excluded from the source modelling. The range of admissible rupture scenarios then needs to be sampled evenly to properly scan the parameter space. For example, if one solid blue circle in Fig. 1(a) represents 100 physically acceptable rupture scenarios, we may perform physics-based source and ground motion modelling with those 300 rupture scenarios represented with the solid blue circles, but 100 rupture scenarios represented by the open solid circle are not taken into account in the modelling, which implies that seismic hazard and risk analysis based on these ground motion simulation results may not be complete if the next event happens from the open blue circle, and it produces much different ground motion characteristics from events from the solid blue circles. It is very challenging to cover the entire range of physically plausible rupture models for scenario events especially when we are limited in fully understanding earthquake source process. However, even given a subset of physics-based source models, it greatly helps to sample the space efficiently if we have a consistent statistical framework that governs the target physics-based source models.

We may assign non-uniform probability to the range of physically acceptable rupture scenarios (Fig. 1b), depending on the level of knowledge and information about target source models. In other words, we quantify the variability and relative likelihood of rupture scenarios within the non-zero probability region. If we could predict every aspect of the rupture process in a future event in a fully deterministic sense, the probability density function (PDF) in Fig. 1(b) would become the Dirac delta function. The earthquake rupture process is a high-dimensional problem, but we adopt a univariate domain to illustrate the efficiency of developing a statistical framework in finite source modelling.

Song & Somerville (2010) and Song & Dalguer (2013) propose to characterize the rupture process in the framework of 1-point and 2-point statistics. As illustrated in Fig. 2, we assign one random field to each source parameter. For example, $X(\mathbf{u})$ is assigned to slip at location, $\mathbf{u}$, and $Y(\mathbf{u})$ is assigned to rupture velocity at location $\mathbf{u}$. If we consider a fault plane discretized in $M \times N$ subfaults, then there are $M^*N$ random variables for each source parameter. If we consider $p$ source parameters, we may need to constrain a $p^*M^*N$ dimensional PDF to define the random field model. In practice, however, we are often limited to constraining 1-point and 2-point statistics. 1-point statistics represents each marginal PDF (mPDF) from the original multivariate PDF. In other words, it controls the variability of each source parameter at any given subfault patch. A classical

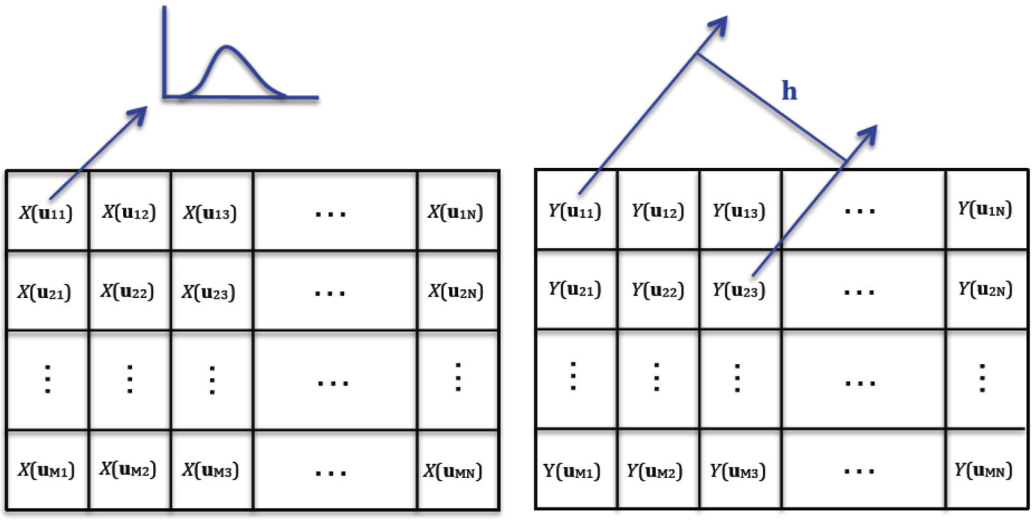


**Figure 2.** 2-D distribution of random variables assigned to each source parameter on a planar fault, that is, $X(\mathbf{u}_{ij})$ and $Y(\mathbf{u}_{ij})$ are random variables that represent one of source parameters, such as slip, rupture velocity, slip velocity and slip duration. $\mathbf{u}_{ij}$ is a location vector and $\mathbf{h}$ is a separation vector between two random variables. Random variables, $X$ and $Y$, have their own univariate (1-point) probability density function (PDF) at a given subfault patch, and 2-point correlation structures can also be inferred as a function of $\mathbf{h}$ (fig. 4 in Song & Dalguer (2013)).

form of empirical ground motion prediction equation (GMPE) is a good example of 1-point statistics in ground motion prediction because the variability of ground motion intensity measures at any given location (or at any given source-to-site distance) are defined by the median and standard deviation in the log-normal distribution. 2-point statistics comprises autocorrelation in the spatial distribution for a single parameter, and cross-correlation between source parameters, which can be implemented in the covariance (or correlation) matrix of the multivariate Gaussian PDF. See also Song & Somerville (2010) and Song & Dalguer (2013) for more details.

### 2.2 1-point and 2-point statistics in dynamically generated source models

1-point and 2-point statistics of earthquake source parameters, defined in Section 2.1, are generally not well constrained despite increased numbers of finite source rupture images of past events. The scaling of mean slip with earthquake size has been relatively well studied (Somerville *et al*. 1999; Mai & Beroza 2000). The power spectrum of slip distribution (2-point autocorrelation of slip) is also constrained by kinematic source models (Somerville *et al*. 1999; Mai & Beroza 2002). Lavallee & Archuleta (2003) and Lavallee *et al*. (2006) examined 1-point statistics of earthquake slip from kinematic source models, while Song *et al*. (2009) investigated cross-correlation structures from kinematic source models. Graves & Pitarka (2010) adopted empirical relations, constrained by previous studies, to derive temporal source parameters in source modelling.

Earthquake source models generated from dynamic rupture simulations may help to constrain the 1-point and 2-point statistics of earthquake ruptures, which can then be used to build a new stochastic modelling approach. Dalguer & Mai (2011, 2012) simulated 360 dynamic rupture models, with varying faulting style and under different normal stress conditions, assuming linear slip-weakening friction (Andrews 1976; Day 1982). Their database of simulated earthquakes, in the magnitude range between $M_w$ 5.5 and 7.0, includes three different source mechanisms (normal, reverse, strike-slip), surface-rupturing and buried events, considering both depth-dependent and constant normal stress. Fine space–time sampling in the dynamic rupture calculations ($dx = 0.1$ km; $dt = 0.008$ s) generates high-resolution spatial data of the rupture process, as well as synthetic near-source seismograms, with a nominal maximum resolved frequency up to 3 Hz (Dalguer & Mai 2011, 2012). The hypocentre location varies on the fault for each event, but it is chosen to be on a patch of high pre-stress. Additional parameters for the geometry of rupture models are summarized in Table 1. The top of the subsurface events is placed at 5 km depth. There are 3 km wide buffer zones that surround the targeted rupture dimension (see Table 1). The slip-weakening distance smoothly increases from 0.3 to 5 m in the buffer to ensure smooth rupture termination at the fault edges. The dynamic rupture models and near-source ground motions have been generated using the Support Operator Rupture Dynamics code, developed by Ely *et al*. (2008, 2009). Baumann & Dalguer (2013) evaluated the compatibility of the ground motion generated by dynamic rupture simulations with empirical GMPEs.

Fig. 3 shows one set of kinematic source parameters from this database of dynamic rupture models, for three different types of buried events, for example, normal ($M_w$ 6.5), reverse ($M_w$ 6.7) and strike-slip ($M_w$ 6.6), with depth-dependent normal stress. Since these kinematic source parameters are derived by solving the elasto-dynamic equations of motion with a given initial stress field and friction law, we expect physical self-consistency between the simulated kinematic source parameters. Both 1-point and 2-point statistics can then be extracted from the given source models. Fig. 4(a) shows 1-point statistics extracted from the normal event (Fig. 3a), assuming stationarity in terms of 1-point statistics, which means that a mPDF is the same for each source parameter at any given subfault patch. All three distributions seem to follow a non-Gaussian distribution, especially for slip and peak slip velocity, suggesting general non-Gaussian properties of earthquake source parameters. However, note the strong depth-dependency of 1-point statistics (Fig. 4b), which is particularly pronounced for slip and peak slip velocity. This pattern is also clearly observed in Fig. 5, in which we examine a PDF after dividing rupture area into several layers with depth. We conclude that for source models with strong depth-dependency, incorrect

**Table 1.** Geometric parameters for dynamically derived source models.

| | Normal | Reverse | Strike-slip |
|---|---|---|---|
| Rupture dimension* (length/width) | 24 km/15 km | 24 km/15 km | 30 km/12 km |
| Dip angle | 60° | 45° | 90° |

*The initial rupture area is surrounded by 3-km thick buffer zones that add additional 6 km rupture length in both along-strike and along-dip directions.

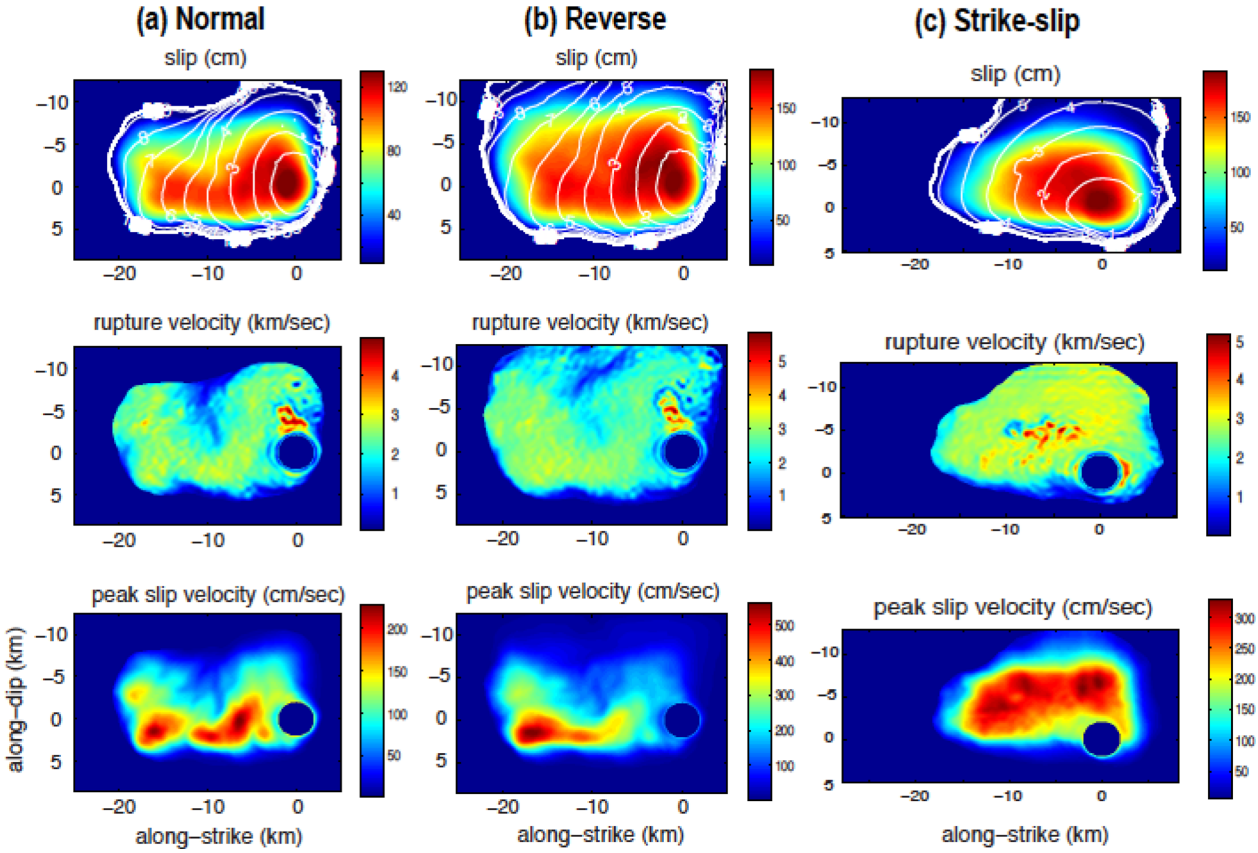


**Figure 3.** Kinematic source parameters derived from dynamic rupture modelling for three target events (Dalguer & Mai 2012). The moment magnitude varies between 6.5 and 6.7 for these events (Normal: $M_w$ 6.5, Reverse: $M_w$ 6.7, Strike-slip: $M_w$ 6.6). The initial nucleation zone and small slip area near the fault boundary are not considered in the following statistical analysis for all source parameters and coloured in dark blue.

statistical inference can follow if stationarity is assumed and only a single PDF for the entire rupture area is inferred (as in Fig. 4a). The depth-dependency of 1-point statistics for certain source parameters reflects the depth-dependency of normal stress assumed in dynamic modelling. It may be realistic since the normal stress, consequently frictional strength, is expected to change with depth and it may also be constrained by investigating kinematic source models for past events. 1-point statistics extracted from two other events (e.g. reverse and strike-slip) in Fig. 3 are presented in Figs S1–S4.

We also extract the 2-point auto- and cross-correlation structures from the same event (Fig. 6). Autocorrelation structures are more elongated in the along-strike direction for slip and peak slip velocity, while they are more elongated in the along-dip direction for rupture velocity. We also detect significant correlations between all three pairs of source parameters. Points of maximum correlation are located at or near zero-offset points for this rupture. The cross-correlation structures are also elongated in the along-strike direction. 2-point correlation structures for other two events (e.g. reverse and strike-slip) are presented in Figs S5 and S6.

To obtain an overall understanding of the possible correlation structure in such dynamic rupture models, we extract 2-point statistics from 203 events ($6.5 \leq M_w \leq 7.0$) in the database, excluding 157 events with $M_w < 6.5$ for the data set of 360 events, since the chosen artificial initial nucleation may affect the rupture process of small-to-moderate size events more strongly. The cross-correlation coefficients extracted from the 203 events reveal strong correlation between all three pairs of source parameters (Fig. 7a). We do not claim that a few hundred events used in our analysis adequately sample the whole space of finite source models, but the emerging correlation structures for the selected number of events is an encouraging fact.

Correlation coefficients at zero-offset points are shown in Fig. 7(b). Although the lower tails are slightly stretched further towards smaller correlation values in Fig. 7(b), there are no significant differences between two panels in Fig. 7, because the correlation maximum points are located near the zero-offset points for most of the 203 source models. As we see in Fig. 8, response distance (RD) is relatively small for most events ($RD < 3$ km). We use the term, RD, defined in Song & Somerville (2010), to provide a

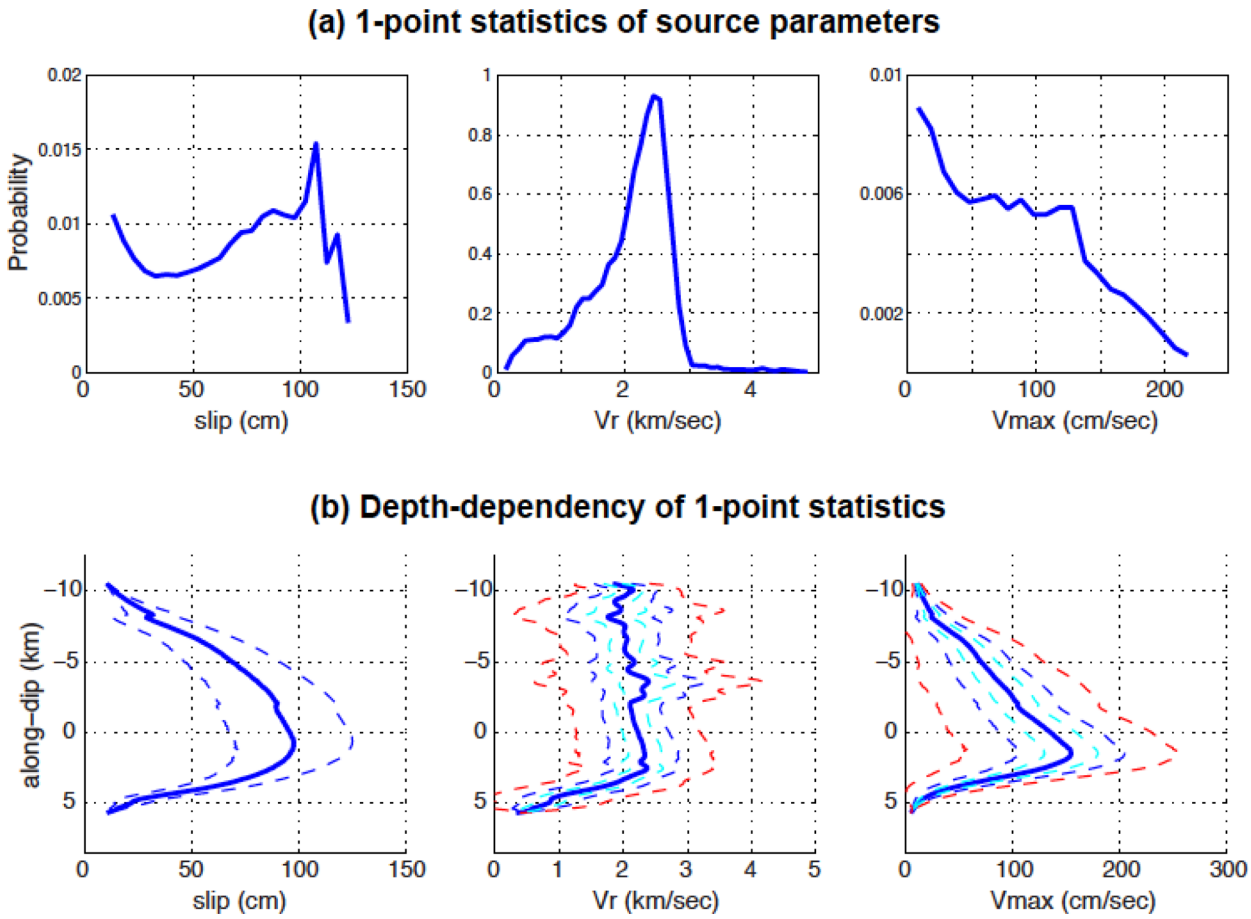


**Figure 4.** 1-point statistics of kinematic source parameters extracted from the normal event in Fig. 3. (a) Marginal probability density function for three-source parameters with stationarity assumption. (b) Depth-dependency of 1-point statistics. The solid and dashed blue lines denote mean and 1-sigma range at the given depth, respectively. The red and cyan dashed lines indicate the perturbation of 1-point statistics we used in ground motion modelling. The red dashed lines indicate that the 1-sigma range (blue dashed lines) is stretched out by a factor of 2 with respect to the solid blue line. The cyan dashed lines indicate that it is compressed by half.

physical interpretation of the lag distance in cross-correlation structures. Due to rupture propagation effects, particularly in long strike-slip events, the lag distance may be relatively large. It may require further studies to confirm the physical origin of the lag distance, but at least for several large strike-slip events, we have observed that this offset distance is quite significant, ∼10 km (Song & Somerville 2010; Song & Dalguer 2013).

## 3 SOURCE MODELLING

Once a finite-fault earthquake source is characterized by a PDF, we can generate a number of rupture scenarios by drawing samples following the target PDF, that is, Monte Carlo sampling. Song & Somerville (2010) propose a sequential Gaussian sampling method with the simple kriging, which is commonly used in the community of geostatistics (Goovaerts 1997; Deutsch & Journel 1998). In this paper, we adopt a stochastic modelling scheme based on the Cholesky factorization of the covariance matrix, constructed by the 1-point and 2-point statistics of kinematic source parameters. A brief description of the stochastic modelling procedure is given in Appendix A. It is important to note that this method aims to reproduce the target 1-point and 2-point statistics, not the entire multivariate PDF. However, we claim that it is still possible to constrain a major portion of the random field model using 1-point and 2-point statistics only.

Stochastic source modelling with the covariance matrix may have several advantages over the Fourier transform-based approaches (Mai & Beroza 2002; Guatteri *et al*. 2004; Liu *et al*. 2006; Bizzarri 2010; Graves & Pitarka 2010; Andrews & Barall 2011). First of all, auto- and cross-correlation structures are implemented in the modelling simultaneously. According to the autocorrelation theorem (Bracewell 2000), the Fourier transform of the autocorrelation function (ACF) is the power spectral density (PSD); therefore, it is equivalent to characterize 2-point autocorrelation either with ACF or with PSD. However, as far as cross-correlation is concerned, we may be in a different situation. If the correlation maximum is shifted from zero-offset point, the corresponding information is not reflected in the amplitude spectrum, but in the phase spectrum. This implies that we cannot characterize certain types of cross-correlation structures by considering only the amplitude spectrum. In contrast, in our proposed stochastic modelling approach, both auto- and cross-correlation structures for all source parameters are jointly implemented in the covariance matrix. In addition, our modelling approach does not require regular grid spacing, which may be useful in case finer gridding near the Earth surface is required. Moreover, it does not require stationarity (appendix D in Song & Somerville (2010)), hence different correlation structures can be

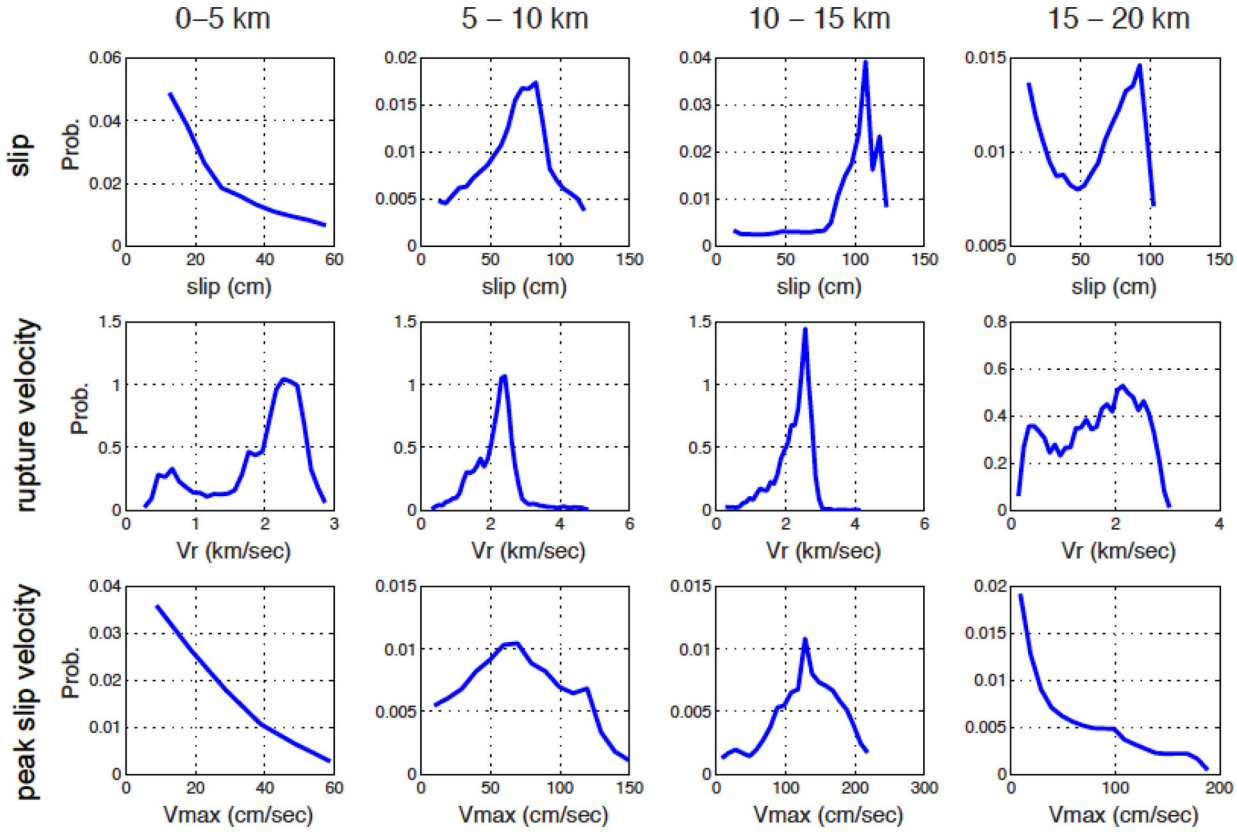


**Figure 5.** Marginal probability density functions (mPDF) obtained for four different depth ranges for the normal event in Fig. 3. Note that the mPDF changes significantly with depth.

applied to different parts of the faulting area. The discrete Fourier transform assumes regular gridding and stationarity in general.

### 3.1 Modelling examples

Once we are given the 1-point and 2-point statistics for a certain event, we generate finite source rupture scenarios by stochastic modelling. Figs 4–6 reveal that the extracted 1-point and 2-point statistics show complex structures, partially due to estimation uncertainty. In this study, we decide to develop a relatively simple statistical model that captures the main characteristics of 1-point and 2-point statistics. We may increase the level of complexity in our target model later. For the 1-point statistics, we assume a Gaussian distribution for all three parameters, and implement depth-dependent mean and standard deviation. For the 2-point statistics, we adopt a simple exponential function as given in eq. (1). We also constrain both correlation length ($a_x$ and $a_z$) and RD ($RD_x$ and $RD_z$) by fitting the exponential function (eq. 1) against empirically obtained auto- and cross-correlation structures (Figs 6, S5 and S6) using an unconstrained non-linear minimization (Nelder–Mead) method:

$$\rho(\mathbf{h}) = \exp\left(-\sqrt{((h_x - RD_x)/a_x)^2 + ((h_z - RD_z)/a_z)^2}\right), \quad \mathbf{h} = (h_x, h_z). \qquad (1)$$

Thus, we have five different model parameters to characterize the 2-point statistics, for example, four parameters in eq. (1) and $\rho_{\max}$ for cross-correlation. Each parameter has six independent components because we consider three source parameters.

Although we extract correlation structures from about 200 events, we decided to work with 3 events presented in Fig. 3 in terms of source and ground motion modelling. While the final goal of our work is to develop a more generalized version of pseudo-dynamic source models, considering a wide range of events, this is beyond the scope of the current study in which we focus on the proof of concept. We also think that it is important to carefully examine the performance of the new modelling approach based on a small set of events, before developing a generalized model. Another simplification in our modelling is to keep the same slip in pseudo-dynamic source models as the one in the dynamic models. In a more general set-up, we may simulate slip heterogeneity, using the autocorrelation structure of earthquake slip. However, constraining slip allows us to more directly investigate how temporal source parameters are controlled in the new pseudo-dynamic source modelling method. One of the major issues in the pseudo-dynamic source modelling is how to link slip with temporal source parameters in kinematic modelling and produce the temporal source parameters compatible with dynamic rupture models (Guatteri *et al.* 2004).

Table 2 shows the five model parameters computed for three events in Fig. 3 for 2-point statistics. We plug them into the rupture model generator (RMG) and simulate the spatial distribution of kinematic source parameters. Fig. 9 shows pseudo-dynamic source models obtained by stochastic modelling for the normal event in Fig. 3. Pseudo-dynamic source models for both reverse and strike-slip events are presented in Figs S7 and S8, respectively. Source models in the left column are derived from spontaneous dynamic rupture modelling; the next three columns show the first three source models generated by stochastic modelling, given the same target 1-point and 2-point statistics. In total, we simulate 30 pseudo-dynamic

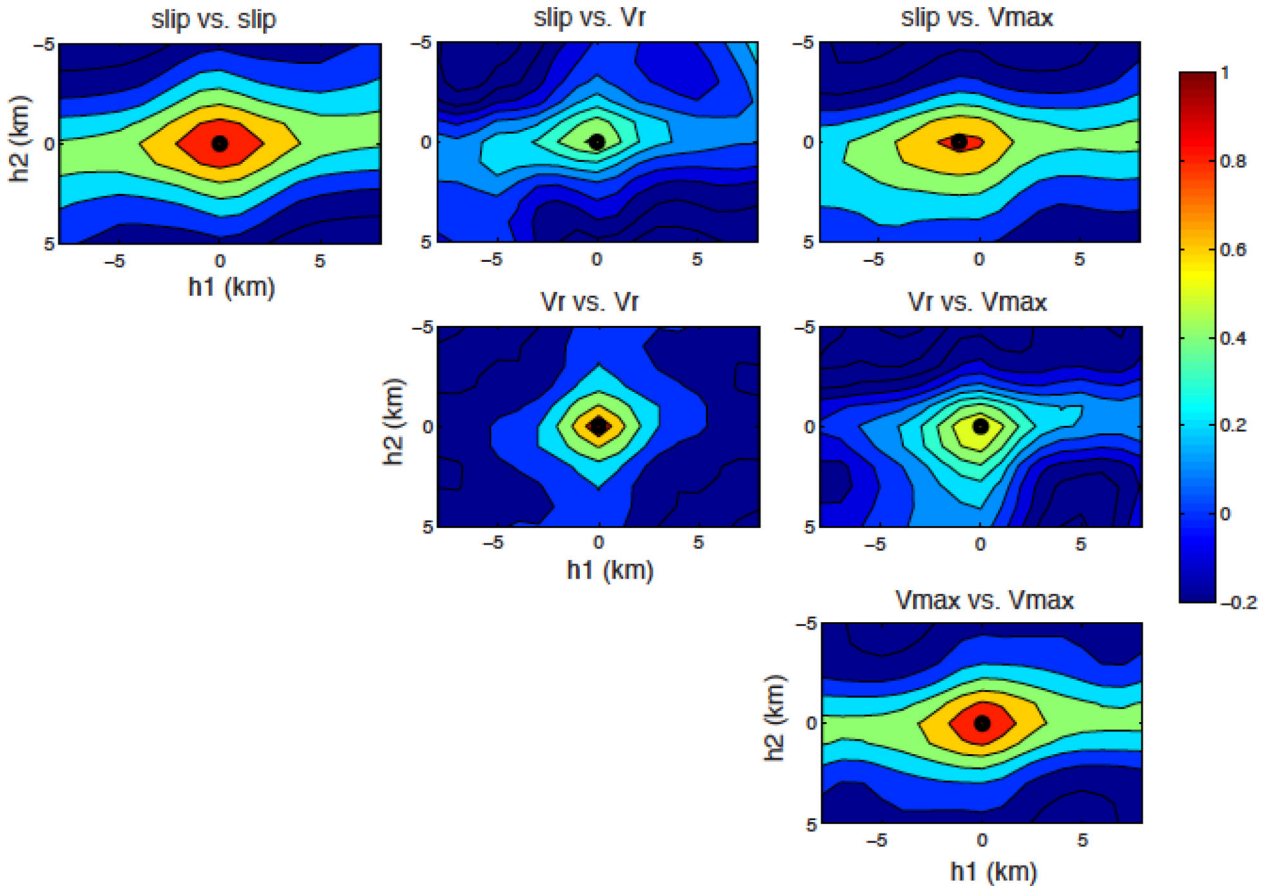


**Figure 6.** 2-point correlation structure extracted from the normal event in Fig. 3(a). The diagonal blocks indicate the autocorrelation of each source parameter and the off-diagonal blocks indicate the cross-correlation between source parameters.

source models for each type of event, but we display only the first three events. The same hypocentre from the dynamic rupture model is used in pseudo-dynamic source models. We may constrain hypocentre locations in generalized pseudo-dynamic modelling, based on a correlation study between hypocentre and earthquake slip (Mai *et al*. 2005). Stochastic modelling simulates the local rupture velocity, and the corresponding rupture time at each point on the fault plane is then computed using the simulated rupture velocity, assuming a straight line of rupture propagation between the hypocentre and each subfault patch. This approximation is valid if rupture speed variations remain small and localized.

All three rupture models generated by stochastic modelling share certain common features. For example, high and low rupture-velocity zones are approximately colocated between dynamically and pseudo-dynamically generated source models because of positive correlation between them. Peak slip velocity shows high values at the range of 10–15 km in the along-dip direction in both models because of the depth-dependency of 1-point statistics. Overall we observe that, given the fixed slip, we can successfully reproduce temporal source parameters compatible with the ones generated by dynamic modelling, using 1-point and 2-point statistics extracted from the dynamically generated source models. On the other hand, the three pseudo-dynamically generated source models are not identical. They show a certain level of variability, which we may call aleatory uncertainty in source modelling. Although we have complete information about our target 1-point and 2-point statistics, stochastic modelling produces variability for each individual random realization and it cannot be predicted with improved knowledge and data. If we have estimation uncertainty in our 1-point and 2-point statistics, we can call it epistemic uncertainty in pseudo-dynamic source modelling.

## 4 GROUND MOTION MODELLING

We generate three-component synthetic seismograms (effective up to 3 Hz) at 168 locations (Fig. 10) for both the dynamic ruptures and the pseudo-dynamic source models. The pseudo-dynamically generated finite source models are combined with pre-computed Green's functions (Zhu & Rivera 2002). We apply the slip velocity function (SVF) proposed by Liu *et al*. (2006) to characterize the slip-rate evolution at each point on the fault. Other types of SVFs, such as triangular, boxcar, modified Yoffe function (Tinti *et al*. 2005a), can be applied, and will affect the radiated wavefields, but this is beyond the scope of this study.

It is an open question how to validate our pseudo-dynamic source modelling methods. We may compare ground motions generated by pseudo-dynamic source modelling with recorded ground motions for real events, and investigate how closely the pseudo-dynamic method predicts recorded waveforms, at least in a statistical sense. We may also compare pseudo-dynamically generated ground motion data with empirical GMPEs, and investigate how well it reproduces ground motion intensity and their variability. However, this type of validation analysis requires a comprehensive study that covers a wide range of events. Sometimes it is not easy to define objective validation criteria. In this paper, we focus on analysing

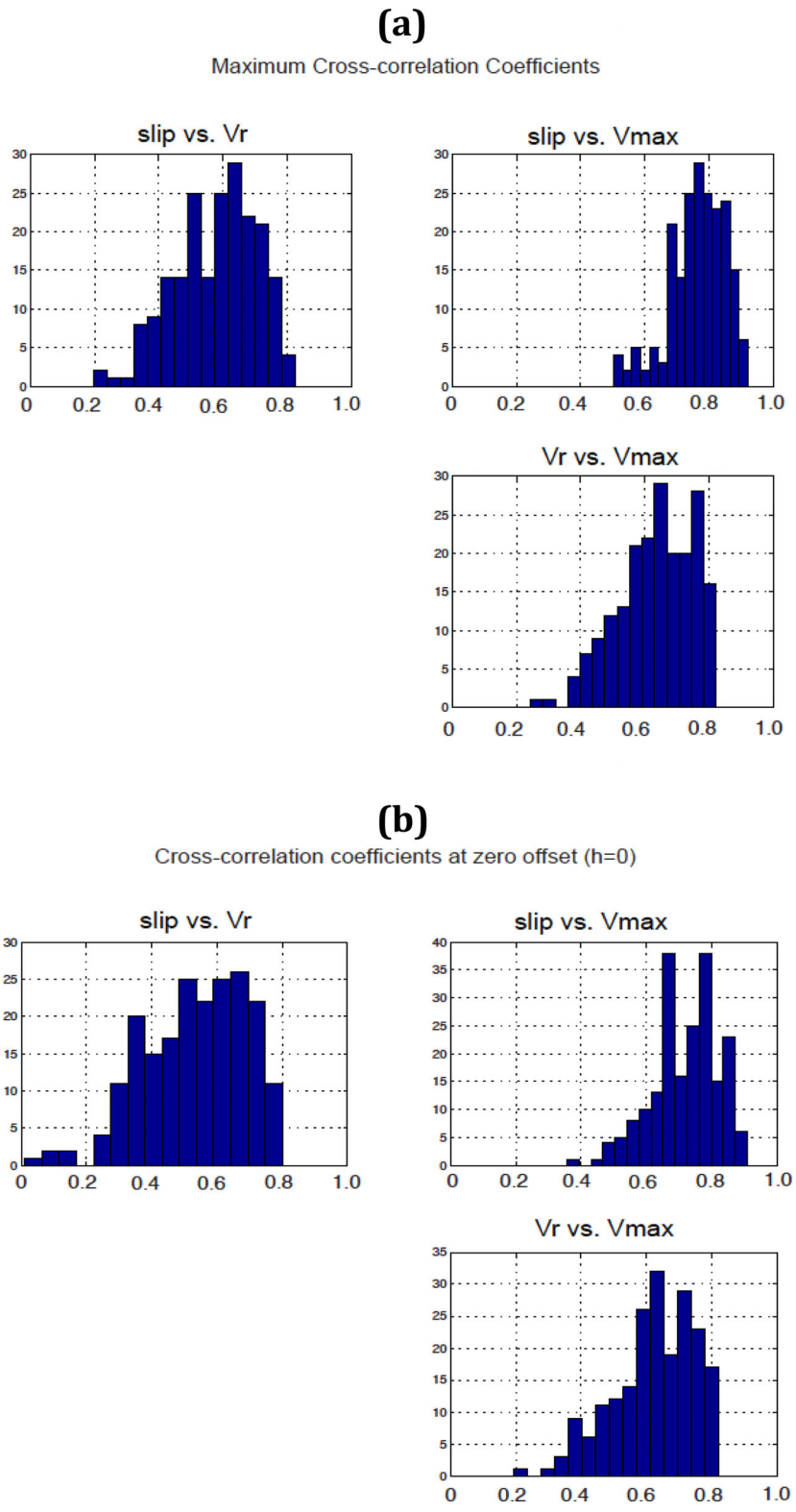


**Figure 7.** Cross-correlation coefficients extracted from 203 events in the dynamic rupture model database. The magnitude ranges between 6.5 and 7.0. The database includes various types of events, such as strike-slip versus dip-slip, surface versus subsurface rupture and depth-dependent versus independent stress field in dynamic modelling. (a) Maximum correlation coefficients, (b) correlation coefficients at zero offset ($h = 0$).

the sensitivity of ground motions to each statistical element of the pseudo-dynamic source model. Once we perturb a certain statistical element in the pseudo-dynamic source model, we will investigate how it affects ground motions. Such a detailed sensitivity analysis will provide more direct physical intuitions about the relations between pseudo-dynamic source parameters and ground motions, which could be used as a basis for more comprehensive validation studies.

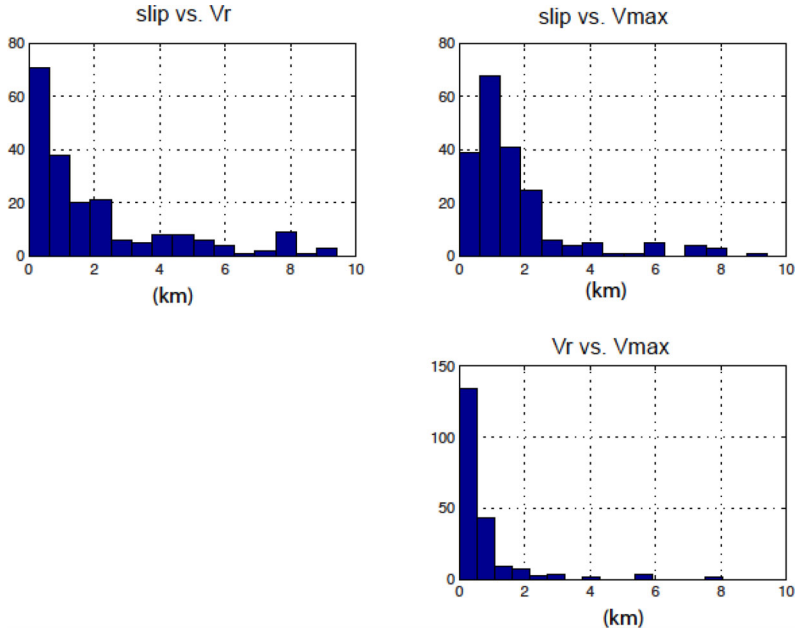


**Figure 8.** Response distance (RD).

**Table 2.** Input parameters for 2-point statistics of three target events.

| | Normal | Reverse | Strike-slip |
|---|---|---|---|
| $a_x$ | $\begin{pmatrix} 11.4 & 3.2 & 11.3 \\ & 0.8 & 4.6 \\ & & 9.6 \end{pmatrix}$ | $\begin{pmatrix} 6.4 & 6.2 & 21.6 \\ & 2.7 & 14.4 \\ & & 12.7 \end{pmatrix}$ | $\begin{pmatrix} 5.8 & 5.7 & 9.3 \\ & 5.4 & 16.3 \\ & & 10.0 \end{pmatrix}$ |
| $a_z$ | $\begin{pmatrix} 1.5 & 1.2 & 1.3 \\ & 2.2 & 0.7 \\ & & 1.2 \end{pmatrix}$ | $\begin{pmatrix} 2.2 & 1.9 & 2.1 \\ & 1.3 & 1.8 \\ & & 2.5 \end{pmatrix}$ | $\begin{pmatrix} 2.0 & 1.1 & 1.4 \\ & 2.1 & 1.9 \\ & & 1.3 \end{pmatrix}$ |
| $\rho_{max}$ | $\begin{pmatrix} 1 & 0.53 & 0.86 \\ & 1 & 0.62 \\ & & 1 \end{pmatrix}$ | $\begin{pmatrix} 1 & 0.63 & 0.73 \\ & 1 & 0.66 \\ & & 1 \end{pmatrix}$ | $\begin{pmatrix} 1 & 0.50 & 0.89 \\ & 1 & 0.61 \\ & & 1 \end{pmatrix}$ |
| $RD_x$ | $\begin{pmatrix} 0 & 0 & -1 \\ & 0 & 0 \\ & & 0 \end{pmatrix}$ | $\begin{pmatrix} 0 & -1 & -2 \\ & 0 & 0 \\ & & 0 \end{pmatrix}$ | $\begin{pmatrix} 0 & 0 & -1 \\ & 0 & 0 \\ & & 0 \end{pmatrix}$ |
| $RD_z$ | $\begin{pmatrix} 0 & 0 & 0 \\ & 0 & 0 \\ & & 0 \end{pmatrix}$ | $\begin{pmatrix} 0 & 0 & 1 \\ & 0 & 0 \\ & & 0 \end{pmatrix}$ | $\begin{pmatrix} 0 & -1 & -1 \\ & 0 & 0 \\ & & 0 \end{pmatrix}$ |

*Note:* Unit for all parameters except $\rho_{max}$ is killometres. And all matrices should be symmetric.

We generate 30 earthquake scenarios by stochastic modelling for each target event in Fig. 3, to account for the aleatory uncertainty in source modelling. Since we consider three dynamically generated source models (e.g. normal, reverse, strike-slip), there are in total 90 pseudo-dynamically generated source models, given the target 1-point and 2-point statistics (Figs 4, 6, S1, S3, S5 and S6). In addition, we construct seven new sets of pseudo-dynamic source models that are linked to perturbation of 1-point statistics, and seven new sets that are linked to perturbation of 2-point statistics. So we have 1350 pseudo-dynamically generated source models ($= 90 \times (14 + 1)$), including the original pseudo-dynamic source model. Then we compare ground motions generated from all 15 sets of pseudo-dynamic source models in a statistical sense. Note that all these pseudo-dynamic rupture models are constructed using the stochastic parameters listed in Table 2.

Fig. 11 shows ground motions obtained by both dynamic and pseudo-dynamic source modelling at five selected points (Fig. 10). We observe that pseudo-dynamically generated ground motions quite well reproduce the dynamically generated ground motions. Since our stochastic modelling generates temporal source parameters of the pseudo-dynamic source models, we do not expect that the former fit the latter completely, in a deterministic sense. The difference in the three waveforms in colour (red, blue and green) indicate variability in ground motions caused by variability in three pseudo-dynamic source models in Fig. 9. The variations in the resulting ground motions seem to remain small at all five locations. This implies that 1-point and 2-point statistics are relatively strong constraints in the random field model. Thus, if we fix one source parameter (e.g. slip in Fig. 9), we can control the other parameters in a very narrow range of random model space with the conditional PDF, constructed from the given 1-point and 2-point statistics and the fixed parameter.

We now compare dynamically generated ground motions with pseudo-dynamically generated ground motions after perturbing the 1-point and 2-point statistics. We compute the difference of peak ground velocity (PGV) in natural log-scale at the 168 stations, compute the corresponding mean and standard deviation and average over 30 randomly simulated events. This procedure combines both intraevent and interevent variability. If the computed mean is above 0, the pseudo-dynamically generated PGVs are on average larger than, and hence overpredict, the dynamically generated PGVs. If it is below 0, the former underpredicts the latter. The standard deviation reveals whether this pattern of over- and underprediction is consistent for all stations. For example, if pseudo-dynamically generated ground motions overpredict dynamically generated ground motions by 50 per cent at all stations uniformly, the standard deviation will be zero although the mean is 0.4 ($= \ln(1.5)$). On the other hand, the standard deviation can be large if the pattern of over- and underprediction changes significantly station by station, while the mean may still be close to zero.

*Perturbation of 1-point statistics:* Using dynamic rupture modelling with multiple set of initial random stress, Song & Dalguer (2013) demonstrate that the standard deviation of source parameters might affect near-source source ground motion characteristics significantly. However, the standard deviation of most source

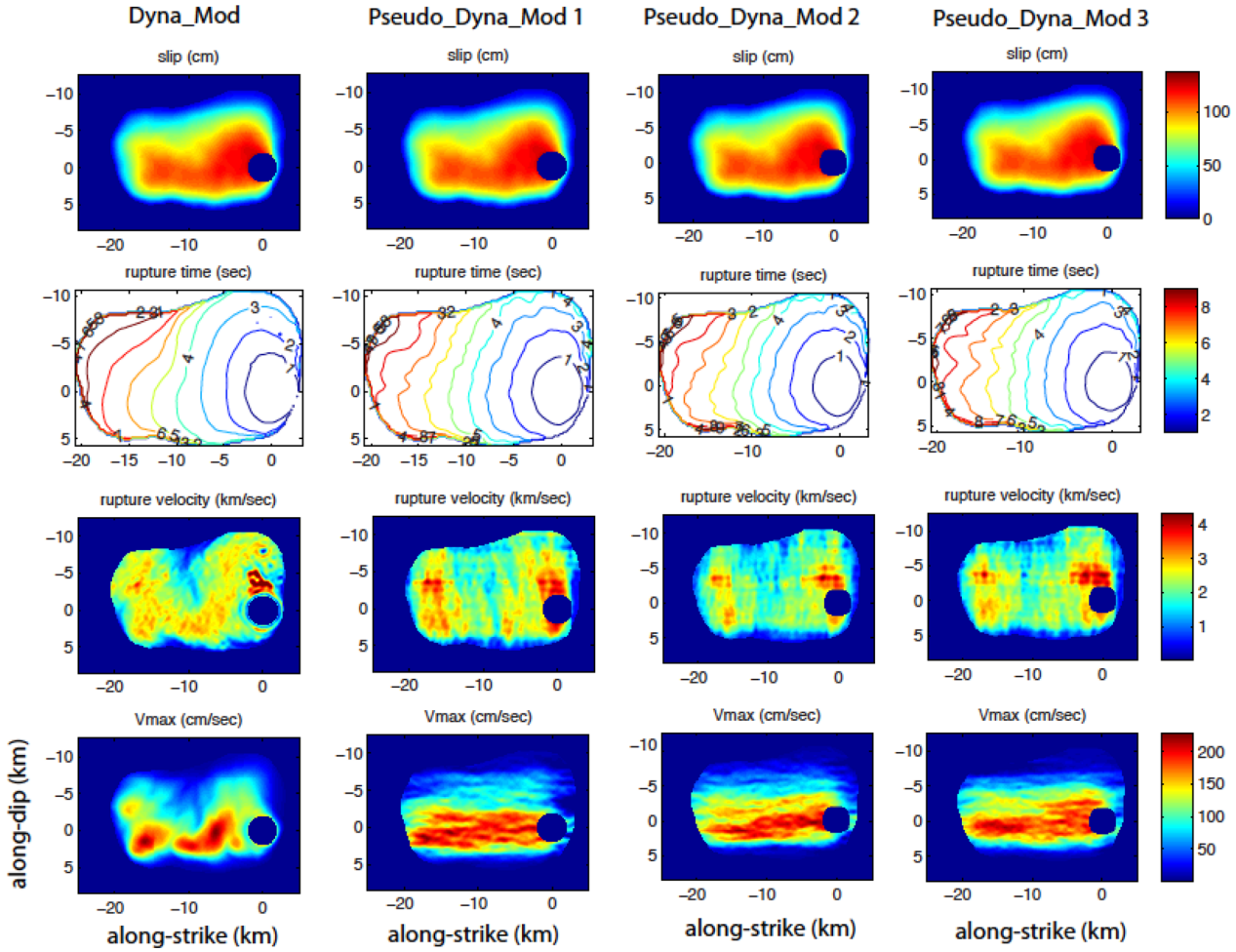


**Figure 9.** Pseudo-dynamic source models obtained from stochastic modelling with given 1-point and 2-point statistics for the normal event in Fig. 3(a). The first column shows dynamically generated kinematic source parameters from Fig. 3(a). The next three columns show three different pseudo-dynamic source models produced given the same 1-point and 2-point statistics. We may consider it aleatory uncertainty in source modelling.

parameters is still poorly constrained by data, and rarely considered explicitly in most source-modelling studies. To address this problem, we perturb the depth-dependent standard deviation of both rupture velocity and peak slip velocity (Fig. 4b), and regenerate seven different sets of pseudo-dynamic source models. Six of them are generated by increasing or decreasing the standard deviations of both temporal source parameters by a factor of 2, as illustrated with red and cyan dashed lines in Fig. 4(b). We also generate a pseudo-dynamic source model by removing the depth-dependency of the 1-point statistics and adopting averaged mean and sigma for the entire rupture area, irrespective of depth. Both depth-dependent mean and standard deviation of earthquake slip and depth-dependent mean of rupture velocity and peak slip velocity remain unchanged for this set of seven pseudo-dynamic source models. 2-point statistics, that is, auto- and cross-correlation matrices, are also kept the same. Several pseudo-dynamic source models are presented in Fig. S9 after perturbing their 1-point statistics. If we increase the standard deviation, data values above and below mean are stretched in opposite directions. Since higher peak values occur after these perturbations, we expect significant changes in the resulting ground motion intensities, particularly in terms of their peak values near the source.

We present ground motion waveforms obtained by different types of perturbation of 1-point statistics at five selected points (Fig. S10). Fig. 12 shows the three components of ground motion for the modelling results with eight different versions of pseudo-dynamic source models after the perturbation of 1-point statistics. Fig. 12(a) reveals that an increase in the standard deviation of temporal source parameters produces stronger ground motions (red and magenta), compared to ground motions (blue line) generated by the original pseudo-dynamic source model. Decrease in the standard deviation generates weaker ground motions (green and cyan). It is interesting to see that pseudo-dynamic source model with depth-independent 1-point statistics produce weaker ground motions (black line). However, we do not observe a clear pattern in terms of standard deviation after perturbing 1-point statistics. This experiment shows that larger standard deviation of source parameters produces stronger peak ground motions. Given the fact that the 1-point variability of source parameters is poorly constrained, our results strongly suggest that the 1-point variability of source parameters deserves more attention in finite source modelling.

*Perturbation of 2-point statistics:* It is even more interesting to compare ground motions after perturbing 2-point statistics. Fig. 13 shows several examples of the correlation structure after perturbation of 2-point statistics. Fig. 13(a) shows the original correlation matrix used in producing pseudo-dynamic models (Fig. 9). We may remove all cross-correlation structures (Fig. 13b), or we may keep some of them and remove others (Figs 13c and d). Since we have

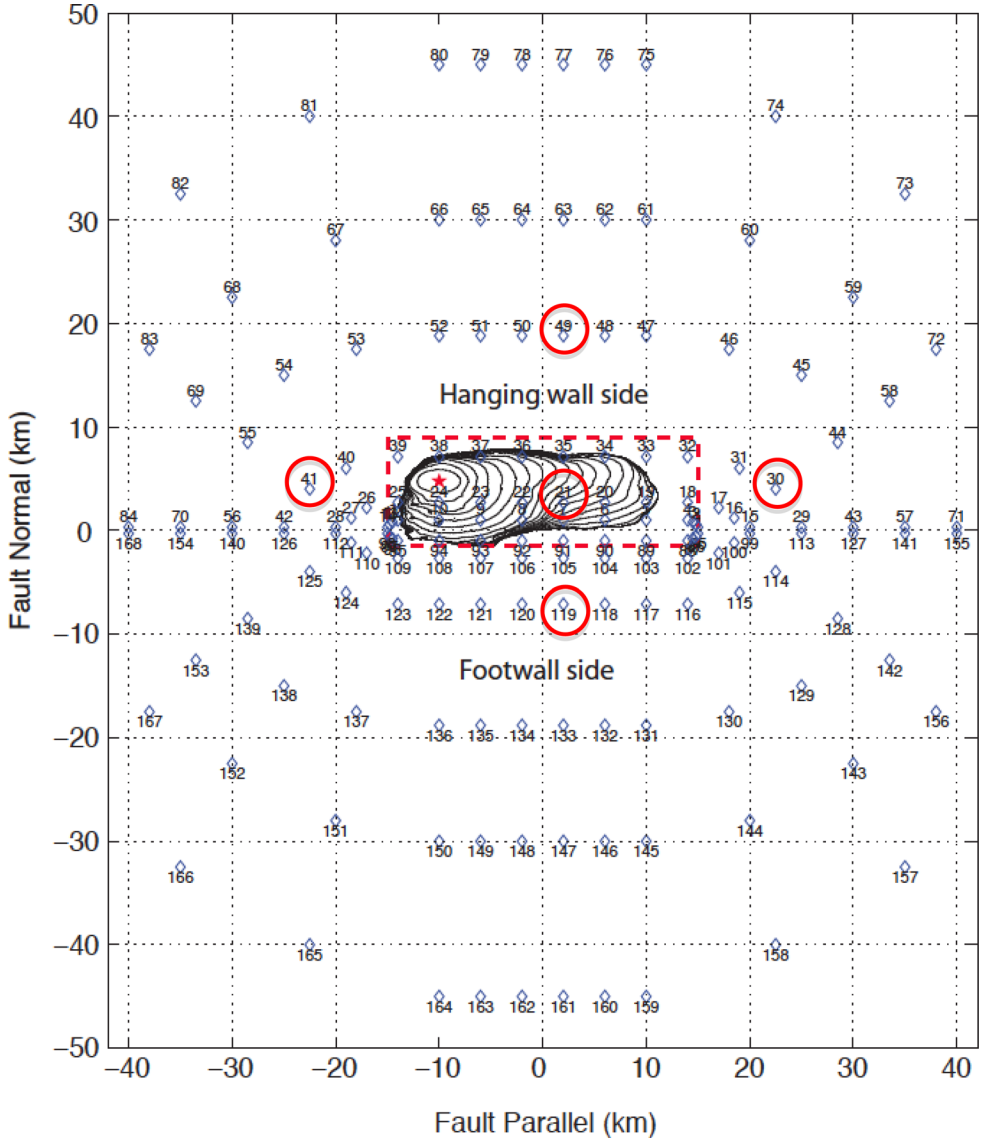


**Figure 10.** The location of 168 stations with the surface projection of the rupture dimension of one target event. Red circles indicate five selected stations, whose waveforms are shown in Fig. 11.

three cross-correlation structures, we have eight different sets of cross-correlation matrices as labelled in Fig. 14. The corresponding autocorrelation matrices (diagonal blocks in Fig. 13) and 1-point statistics are retained while perturbing cross-correlation matrices.

We present several pseudo-dynamic source models and corresponding ground motion waveforms at the five selected stations in Figs S11 and S12, respectively, after the perturbation of 2-point statistics. Fig. 14 clearly shows that correlation produces stronger ground motions. Interestingly, we observe two separate types of ground motion behaviour, especially for dip-slip events. Once we include the correlation between slip and rupture velocity (red and magenta), they are grouped together with the blue line. If we do not include it, it is grouped with the black line. This pattern may tell us something about how each component of the cross-correlation matrix shapes ground motion characteristics. The group with the blue line also shows smaller standard deviation as shown in Fig. 14(b), implying that the prediction pattern of pseudo-dynamic source models could be less random if correlations are included. This sensitivity analysis of ground motions to each element of 1-point and 2-point statistics of source parameters will help to understand the effect of finite source process on near-source ground motion characteristics more quantitatively and systematically.

## 5 DISCUSSION

The statistical framework for finite source modelling proposed in the paper can be considered either pseudo-dynamic RMG or extended earthquake rupture forecast model. The former is linked to earthquake source physics, and the latter is linked to statistical seismology and probabilistic seismic hazard analysis. We emphasize that these two viewpoints are closely related, and in fact complement each other efficiently. Physics-based source modelling has already been used in simulation-based seismic hazard analysis (Graves *et al.* 2011), enabling us to select rupture scenarios in the non-zero probability area in Fig. 1(a). However, this approach may still not satisfy all additional requirements to fully quantify the variability of finite source models as addressed in Fig. 1.

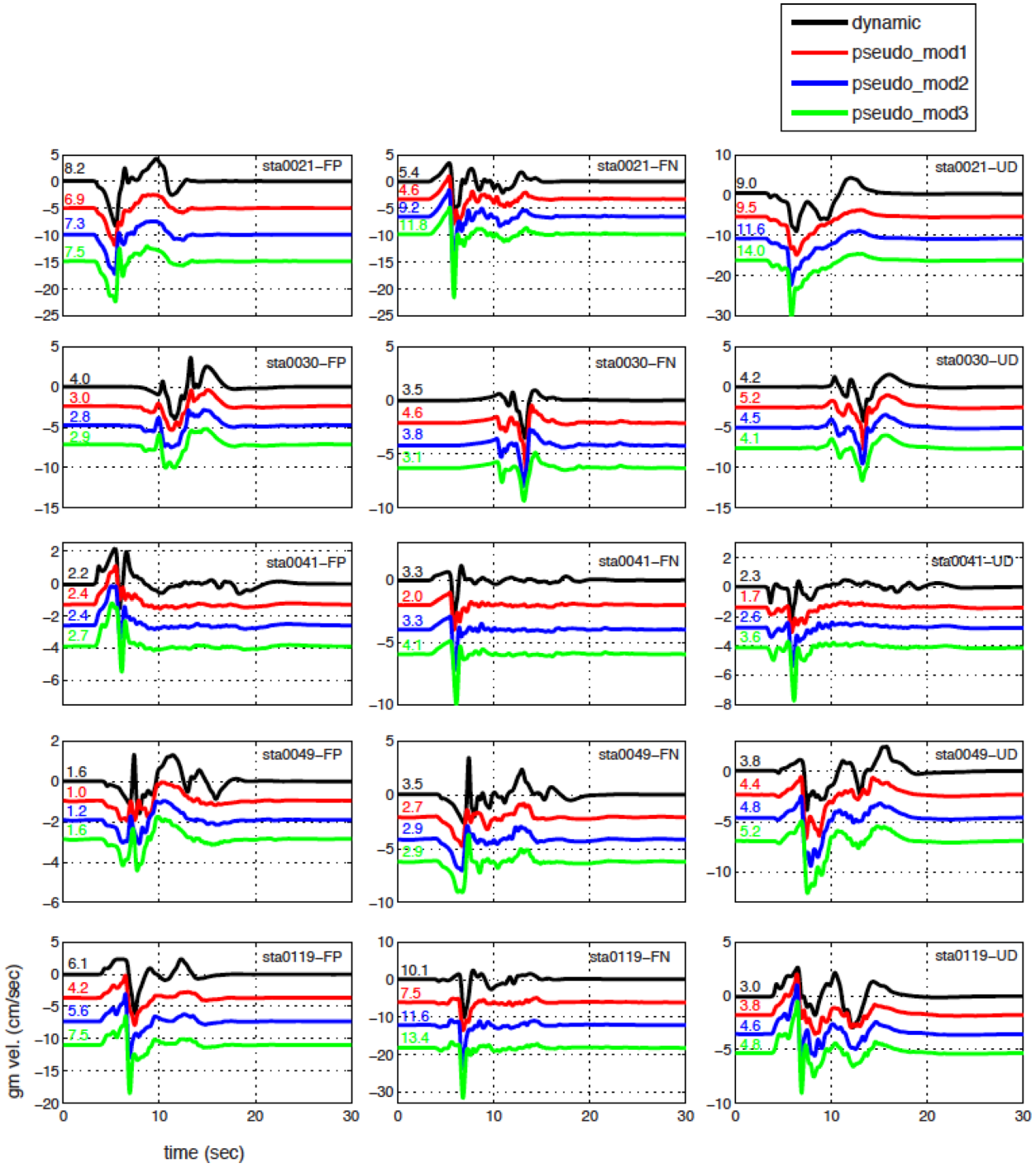


**Figure 11.** Comparison of waveforms obtained by both dynamic and pseudo-dynamic modelling at five selected stations in Fig. 10. Three different waveforms (in colour) are generated by three pseudo-dynamic source models in Fig. 9. Waveforms are shifted vertically for better visual comparison. Numbers at the beginning of each waveform indicate peak ground velocity (PGV).

This motivates the need for constructing a statistical framework to simulate the finite-fault source process. Our improved understanding about earthquake source physics will help to constrain input parameters better in the stochastic model.

The sensitivity analysis of ground motions to each statistical element of the pseudo-dynamic source modelling helps to quantify the effect of earthquake source on ground motions. We find that larger standard deviation and correlation between source parameters produce stronger peak ground motions (Figs 12a and 14a). In particular, the sensitivity analysis with perturbations in the cross-correlations efficiently demonstrates the effect of source parameter correlations on ground motions. We expect that fully correlated kinematic source parameters produce coherent source radiation, consequently stronger ground motions. On the contrary, less correlated source parameters produce less coherent rupture behaviour, and hence weaker ground motions (Olsen *et al*. 2009). We may need a more comprehensive study that includes the number of dynamic source models (203 events in Fig. 7). However, even initial tests

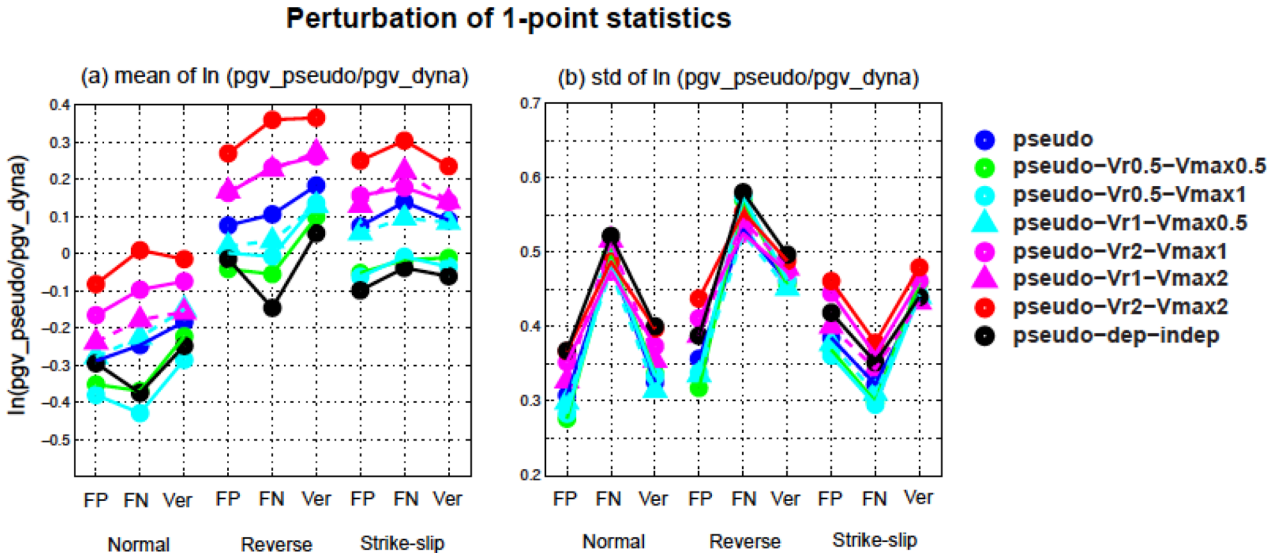


**Figure 12.** Comparison of pseudo-dynamically generated ground motions against dynamically generated ground motions after perturbing a certain element of 1-point statistics in pseudo-dynamic source models. (a) Mean of ln(pgv_pseudo/pgv_dyna) for 168 stations, (b) Standard deviation of ln(pgv_pseudo/pgv_dyna) for 168 stations. Mean and standard deviation are also averaged for 30 randomly simulated events by stochastic modelling.

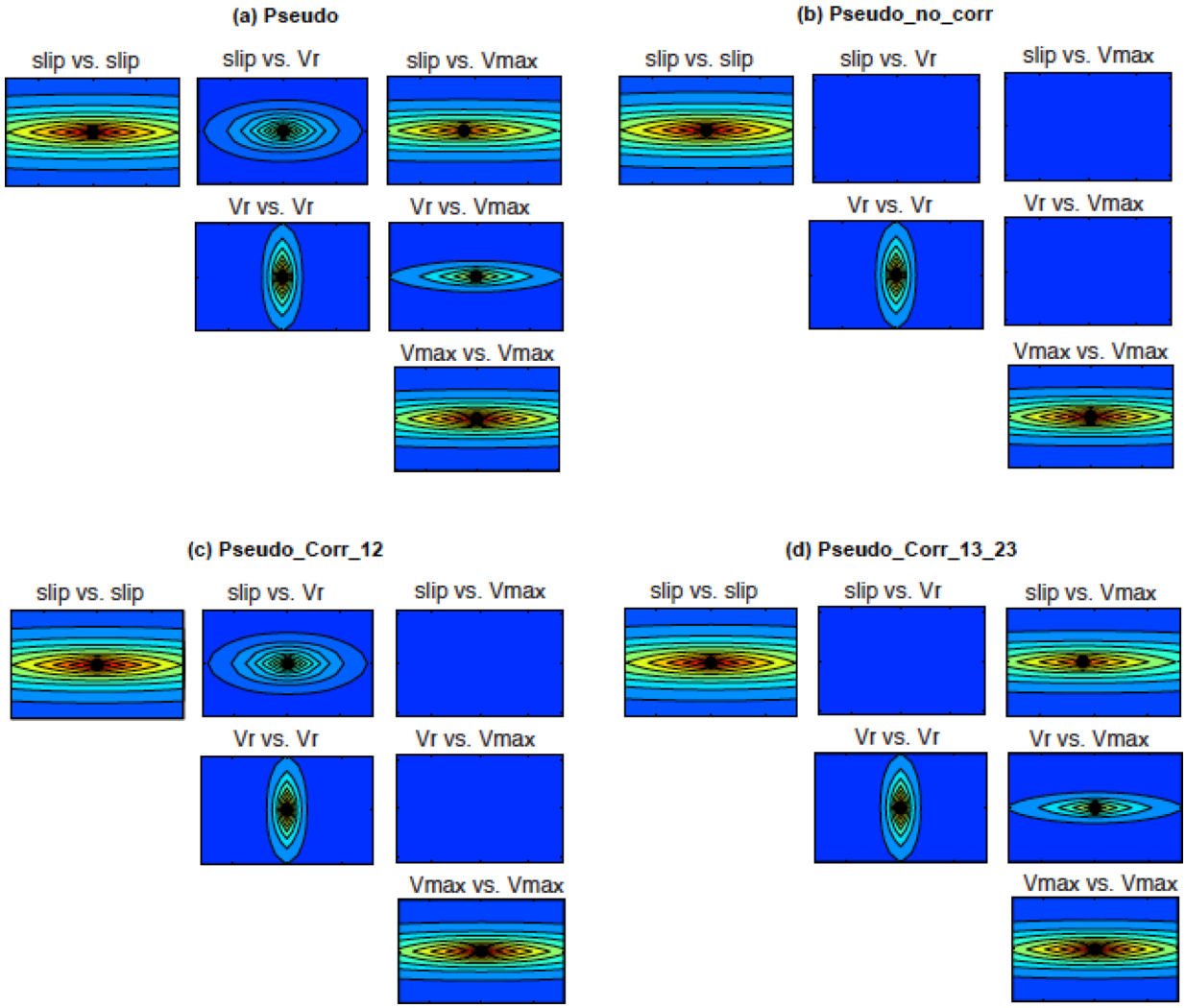


**Figure 13.** Perturbation of 2-point statistics. Three off-diagonal blocks are perturbed sequentially.

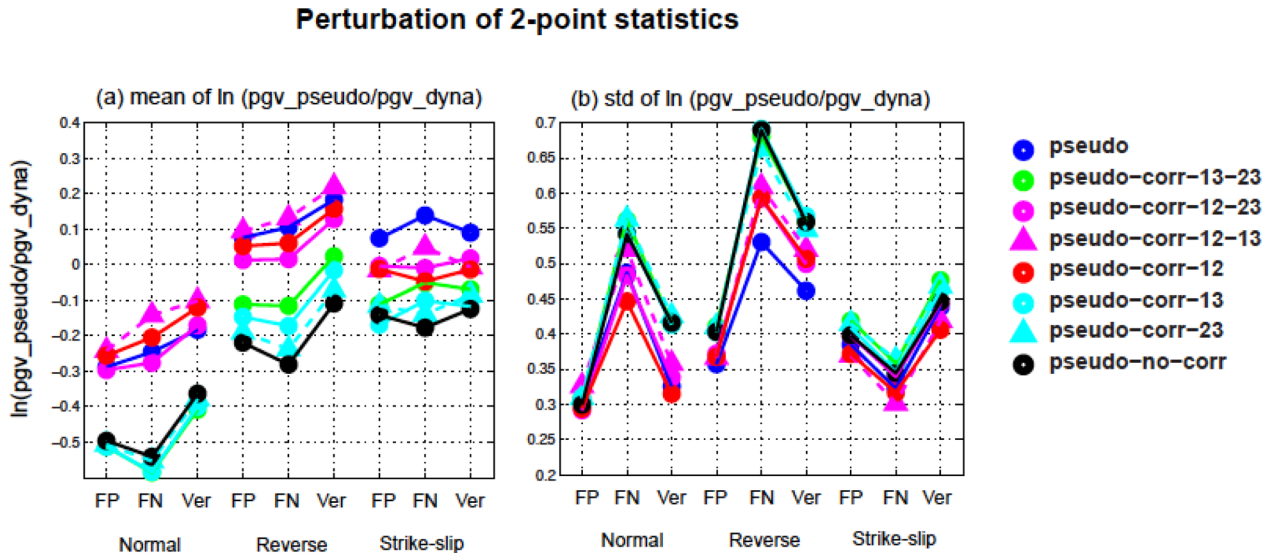


**Figure 14.** Comparison of pseudo-dynamically generated ground motions against dynamically generated ground motions after perturbing a certain element of 2-point statistics in pseudo-dynamic source models. (a) Mean of ln(pgv_pseudo/pgv_dyna) for 168 stations, (b) Standard deviation of ln(pgv_pseudo/pgv_dyna) for 168 stations. Mean and standard deviation are also averaged for 30 events.

with three target events in Fig. 3 efficiently illustrate the effect of 1-point and 2-point statistics of source parameters in ground motion modelling.

Although we successfully demonstrate the efficiency of the new pseudo-dynamic source modelling method with three events in Fig. 3, our final goal is to develop a pseudo-dynamic source model that covers the entire range, or at least a wider range of model space, as conceptually illustrated in Fig. 1. This pilot study considers 203 events in Fig. 7, but we will expand our source model space, considering, for example, different friction laws, stress regimes, complex fault geometry, etc., in dynamic modelling. We may also analyse existing kinematic source models of past events if they are sufficiently well resolved. In this generalization procedure, one of the main issues we need to address is whether there are consistent structures of source statistics (1-point and 2-point statistics) for a wide range of events, or whether we can at least classify them into several different categories. If the source statistics fluctuate significantly for each type of events, it may be more difficult to derive a narrow range of random model space in Fig. 1.

This study utilizes low-frequency ground motion intensity measures, for example, PGV. We plan to generate high-frequency (HF) ground motions in following studies, using the heterogeneity of source parameters produced by target 1-point and 2-point statistics in a similar way. Pulido & Dalguer (2009) generate HF ground motions with kinematic source models, derived from dynamic rupture modelling, assuming that the HF ground motions are generated from abrupt changes of rupture speed (Madariaga 1977). In particular, it would be interesting to investigate a frequency-dependent response of ground motions to each statistical element of our pseudo-dynamic source modelling approach. We may also need to consider more fine detailed structure of 1-point and 2-point statistics at this stage, including non-Gaussian 1-point statistics and additional correlation models for 2-point statistics.

Since most parameters in the framework of 1-point and 2-point statistics are poorly constrained by data, it remains a challenging task to construct a stochastic model in which all components are adequately characterized. Dynamic rupture modelling provides good resources for constraining certain aspects of 1-point and 2-point statistics, in particular, cross-correlation structures (Schmedes *et al*. 2010; Song & Somerville 2010). It is also helpful to investigate the relations between 1-point and 2-point statistics of earthquake source and ground motions in dynamic modelling (Song & Dalguer 2013). Future work will include the correlation structures from dynamic rupture modelling that have been constrained by kinematic source inversion results (Tinti *et al*. 2005b; Causse *et al*. 2013). Additional constraints between kinemetic and dynamic source parameters may be derived from theoretical arguments of fracture mechanics (e.g. Gabriel *et al*. 2012, 2013), although these are likely to provide only general relations and upper/lower bounds, but not the spatial characteristics of rupture parameters.

There are several advantages of covariance matrix-based stochastic source modelling over the Fourier transform-based approaches. However, one technical difficulty in covariance matrix-based methods is to ensure a positive-definite covariance matrix, (e.g. Goovaerts 1997; Song & Somerville 2010). If the covariance matrix is not positive definite, the Cholesky factorization cannot be applied. Here, we resolve this problem by performing an eigenvalue decomposition to remove the negative eigenvalues. However, the additional step of eigenvalue decomposition increases the computational demands if the covariance matrix is large. A potential avenue for a computationally more efficient source modelling approach could be devised by applying a coregionalization technique (Goovaerts 1997).

## 6 CONCLUSIONS

We demonstrate that finite-fault earthquake ruptures can be efficiently characterized by 1-point and 2-point statistics of kinematic source parameters. We develop a stochastic source modelling method to generate a number of rupture scenarios, following a certain target 1-point and 2-point statistics. This covariance matrix-based source modelling method has several advantages over Fourier transform-based approaches. Finite source modelling with 1-point and 2-point statistics enables us to better quantify earthquake source effects on near-source ground motion characteristics. In our ground motion sensitivity analysis, we show that both larger standard

deviation and correlation between source parameters produce stronger peak ground motions. We also find that appropriate consideration of correlation between source parameters is important in physics-based source modelling to capture ground motion variability. Our proposed statistical framework for generating earthquake rupture scenarios improves simulation-based ground motion prediction, and consequently may help to achieve more accurate seismic hazard analysis, in particular, in the near-source region of moderate-to-large earthquakes where data constraints, and hence ground motion prediction schemes, are limited.

## ACKNOWLEDGEMENTS

We thank two anonymous reviewers and the associate editor, E. Fukuyama, for their thoughtful reviews. This study was funded by the NERA project (Network of European Research Infrastructures for Earthquake Risk Assessment and Mitigation) from the 7th Framework Program by the European Commission and the Swiss National Science Foundation (SNF), SNF Grant 200021–140459. Simulations were done at the Swiss National Supercomputing Center (CSCS), under the production projects, 'Development of Dynamic Rupture Models to Study the Physics of Earthquakes and Near-Source Ground Motion' and 'Development of a Database of Physics-Based Synthetic Earthquakes for Ground Motion Prediction'.

## REFERENCES

Abrahamson, N. *et al.*, 2008. Comparisons of the NGA ground-motion relations, *Earthq. Spectra,* **24,** 45–66.

Andrews, D.J., 1976. Rupture velocity of plane strain shear cracks, *J. geophys. Res.,* **81,** 5679–5687.

Andrews, D.J. & Barall, M., 2011. Specifying initial stress for dynamic heterogeneous earthquake source models, *Bull. seism. Soc. Am.,* **101,** 2408–2417.

Aster, R.C., Borchers, B. & Thurber, C.H., 2005. *Parameter Estimation and Inverse Problems,* Elsevier Academic Press.

Baumann, C. & Dalguer, L.A., 2013. Evaluating the compatibility of dynamic-rupture-based synthetic ground motion with empirical GMPE, *Bull. Seism. Soc. Am.,* in press.

Bizzarri, A., 2010. On the relations between fracture energy and physical observables in dynamic earthquake models, *J. geophys. Res.-Solid Earth.,* **115,** doi:10.1029/2009jb007027.

Bracewell, R.N., 2000. *The Fourier Transform and Its Applications,* McGraw-Hill.

Causse, M., Dalguer, L.A. & Mai, P.M., 2013. Variability of dynamic parameters inferred from kinematic models of past earthquakes, *Geophs. J. Int.,* accepted.

Dalguer, L.A. & Mai, P.M., 2011. Near-source ground motion variability from $M = 6.5$ dynamic rupture simulations, in *4th IASPEI/IAEE International Symposium,* University of California, Santa Barbara, USA.

Dalguer, L.A. & Mai, P.M., 2012. Prediction of near-source ground motion exceeding 1 g at low frequencies (<2 Hz) from $M_w \sim 6.5$ deterministic physics-based dynamic rupture simulations, in *Proceedings of the 15th World Conference on Earthquake Engineering (15WCEE),* Lisbon, Portugal.

Dalguer, L.A., Miyake, H., Day, S.M. & Irikura, K., 2008. Surface rupturing and buried dynamic-rupture models calibrated with statistical observations of past earthquakes, *Bull. seism. Soc. Am.,* **98,** 1147–1161.

Day, S.M., 1982. 3-Dimensional simulation of spontaneous rupture—the effect of nonuniform prestress, *Bull. seism. Soc. Am.,* **72,** 1881–1902.

Deutsch, C.V. & Journel, A.G., 1998. *GSLIB: Geostatistical Software Library and User's Guide,* Oxford University Press.

Ely, G.P., Day, S.M. & Minster, J.-B., 2008. A support-operator method for viscoelastic wave modelling in 3-D heterogeneous media, *Geophys. J. Int.,* **172,** 331–344.

Ely, G.P., Day, S.M. & Minster, J.-B., 2009. A support-operator method for 3-D rupture dynamics, *Geophys. J. Int.,* **177,** 1140–1150.

Gabriel, A.A., Ampuero, J.P., Dalguer, L.A. & Mai, P.M., 2012. The transition of dynamic rupture styles in elastic media under velocity-weakening friction, *J. geophys. Res.-Solid Earth.,* **117**, B09311, doi:10.1029/2012JB009468.

Gabriel, A.A., Ampuero, J.P., Dalguer, L.A. & Mai, P.M., 2013. Source properties of dynamic rupture pulses with off-fault plasticity, *J. geophys. Res.*, **118**, doi:10.1002/jgrb.50213.

Goovaerts, P., 1997. *Geostatistics for Natural Resources Evaluation (Applied Geostatistics Series),* Oxford University Press.

Graves, R. *et al.*, 2011. CyberShake: a physics-based seismic hazard model for Southern California, *Pure appl. Geophys.,* **168,** 367–381.

Graves, R.W. & Pitarka, A., 2010. Broadband ground-motion simulation using a hybrid approach, *Bull. seism. Soc. Am.,* **100,** 2095–2123.

Graves, R.W., Aagaard, B.T., Hudnut, K.W., Star, L.M., Stewart, J.P. & Jordan, T.H., 2008. Broadband simulations for M(w) 7.8 southern San Andreas earthquakes: ground motion sensitivity to rupture speed, *Geophys. Res. Lett.,* **35,** doi:10.1029/2008gl035750.

Guatteri, M., Mai, P.M. & Beroza, G.C., 2004. A pseudo-dynamic approximation to dynamic rupture models for strong ground motion prediction, *Bull. seism. Soc. Am.,* **94,** 2051–2063.

Lavallee, D. & Archuleta, R.J., 2003. Stochastic modeling of slip spatial complexities for the 1979 Imperial Valley, California, earthquake, *Geophys. Res. Lett.,* **30,** doi:10.1029/2002gl015839.

Lavallee, D., Liu, P.C. & Archuleta, R.J., 2006. Stochastic model of heterogeneity in earthquake slip spatial distributions, *Geophys. J. Int.,* **165,** 622–640.

Liu, P.C., Archuleta, R.J. & Hartzell, S.H., 2006. Prediction of broadband ground-motion time histories: hybrid low/high-frequency method with correlated random source parameters, *Bull. seism. Soc. Am.,* **96,** 2118–2130.

Madariaga, R., 1977. High-frequency radiation from crack (stress drop) models of earthquake faulting, *Geophys. J. R. astr. Soc.,* **51,** 625–651.

Mai, P.M. & Beroza, G.C., 2000. Source scaling properties from finite-fault-rupture models, *Bull. seism. Soc. Am.,* **90,** 604–615.

Mai, P.M. & Beroza, G.C., 2002. A spatial random field model to characterize complexity in earthquake slip, *J. geophys. Res.-Solid Earth.,* **107,** doi:10.1029/2001jb000588.

Mai, P.M., Sputich, P. & Boatwright, J., 2005. Hypocenter locations in finite-source rupture models, *Bull. seism. Soc. Am.,* **95,** 965–980.

Mena, B., Dalguer, L.A. & Mai, P.M., 2012. Pseudodynamic source characterization for strike-slip faulting including stress heterogeneity and supershear ruptures, *Bull. seism. Soc. Am.,* **102,** 1654–1680.

Oglesby, D.D., Archuleta, R.J. & Nielsen, S.B., 1998. Earthquakes on dipping faults: the effects of broken symmetry, *Science,* **280,** 1055–1059.

Olsen, K.B., Madariaga, R. & Archuleta, R.J., 1997. Three-dimensional dynamic simulation of the 1992 Landers earthquake, *Science,* **278,** 834–838.

Olsen, K.B. *et al.*, 2009. ShakeOut-D: ground motion estimates using an ensemble of large earthquakes on the southern San Andreas fault with spontaneous rupture propagation, *Geophys. Res. Lett.,* **36,** doi:10.1029/2008gl036832.

Pulido, N. & Dalguer, L.A., 2009. Estimation of the high-frequency radiation of the 2000 Tottori (Japan) earthquake based on a dynamic model of fault rupture: application to the strong ground motion simulation, *Bull. seism. Soc. Am.,* **99,** 2305–2322.

Ripperger, J., Mai, P.M. & Ampuero, J.P., 2008. Variability of near-field ground motion from dynamic earthquake rupture Simulations, *Bull. seism. Soc. Am.,* **98,** 1207–1228.

Schmedes, J., Archuleta, R.J. & Lavallee, D., 2010. Correlation of earthquake source parameters inferred from dynamic rupture simulations, *J. geophys. Res.-Solid Earth.,* **115,** doi:10.1029/2009jb006689.

Shi, Z. & Day, S.M., 2013. Rupture dynamics and ground motion from 3-D rough-fault simulations, *J. geophys. Res.-Solid Earth,* **118,** doi:10.1002/jgrb.50094.

Somerville, P. *et al.*, 1999. Characterizing crustal earthquake slip model for the prediction of strong ground motion, *Seismol. Res. Lett.,* **70,** 59–80.

Song, S.G. & Dalguer, L.A., 2013. Importance of 1-point statistics in earthquake source modelling for ground motion simulation, *Geophys. J. Int.,* **192,** 1255–1270.

Song, S.G. & Somerville, P., 2010. Physics-based earthquake source characterization and modeling with geostatistics, *Bull. seism. Soc. Am.,* **100,** 482–496.

Song, S.G., Pitarka, A. & Somerville, P., 2009. Exploring spatial coherence between earthquake source parameters, *Bull. seism. Soc. Am.,* **99,** 2564–2571.

Tinti, E., Fukuyama, E., Piatanesi, A. & Cocco, M., 2005a. A kinematic source-time function compatible with earthquake dynamics, *Bull. seism. Soc. Am.,* **95,** 1211–1223.

Tinti, E., Spudich, P. & Cocco, M., 2005b. Earthquake fracture energy inferred from kinematic rupture models on extended faults, *J. geophys. Res.-Solid Earth,* **110,** doi:10.1029/2005jb003644.

Zhu, L.P. & Rivera, L.A., 2002. A note on the dynamic and static displacements from a point source in multilayered media, *Geophys. J. Int.,* **148,** 619–627.

## APPENDIX A: STOCHASTIC MODELLING PROCEDURE

(1) Determine a set of macroscopic source parameters, such as magnitude, rupture length/width, hypocentre.

(2) Determine a set of target 1-point and 2-point statistics of kinematic source parameters, that is, mean, standard deviation, correlation length, maximum cross-correlation coefficient, RD.

(3) Construct a covariance matrix ($\Sigma$), based on the target 1-point and 2-point statistics (see Appendix B for details).

(4) Construct a set of random distributions that reproduce the target covariance matrix in (3), by following two-step approaches described below. It is straightforward to show that $\boldsymbol{X}$ follows $N(\mu, \boldsymbol{\sigma})$ if $\boldsymbol{Z}$ follows $N(0, \mathbf{I})$ (see Appendix C for proof):

(a) Perform the Cholesky factorization ($\Sigma = \mathbf{L}\mathbf{L}^T$),

(b) Perform random sampling ($\mathbf{x} = \mathbf{L}\mathbf{z} + \mu$).

(5) Transform 1-point statistics if necessary. Currently, 1-point statistics of source parameters follows the Gaussian distribution because the random sampling in (4) is performed with the assumption of the multivariate Gaussian distribution, but it can be transformed to non-Gaussian distributions. This transform will break the multi-Gaussian distribution, but the target covariance matrix will be preserved as long as the transformed distribution has a monotonically and smoothly increasing cumulative density function. See appendix A in Song & Dalguer (2013) for the transformation of 1-point statistics.

(6) Implement derived kinematic source parameters in a specific form of slip velocity function in order to obtain a complete description of finite source process, that is, spatiotemporal evolution of slip or slip velocity function ($s(\mathbf{u}, t)$, or $\dot{s}(\mathbf{u}, t)$).

## APPENDIX B

Once target auto- and cross-correlations are specified, the covariance matrix, $\boldsymbol{\Sigma}$, is filled as shown in equations below. Let us assume that the covariance matrix, $\Sigma$, contains auto- and cross-correlation structure for two-source parameters. For example, $X$ is assigned to earthquake slip and $Y$ is assigned to rupture velocity, respectively,

$$\Sigma = \begin{pmatrix} \Sigma_{XX} & \Sigma_{XY} \\ \Sigma_{YX} & \Sigma_{YY} \end{pmatrix}, \tag{A1}$$

$\Sigma_{XX}$ and $\Sigma_{XY}$ are filled in this way,

$$\Sigma_{XX} = \sigma_X^2 \begin{pmatrix} 1 & \rho(X(\mathbf{u}_{11}), X(\mathbf{u}_{12})) & \dots & \rho(X(\mathbf{u}_{11}), X(\mathbf{u}_{MN})) \\ \rho(X(\mathbf{u}_{12}), X(\mathbf{u}_{11})) & 1 & \dots & \rho(X(\mathbf{u}_{12}), X(\mathbf{u}_{MN})) \\ & \dots & & \\ \rho(X(\mathbf{u}_{MN}), X(\mathbf{u}_{11})) & \rho(X(\mathbf{u}_{MN}), X(\mathbf{u}_{12})) & \dots & 1 \end{pmatrix}. \tag{A2}$$

Once the separation vector, $\mathbf{h} = \mathbf{u}_{pq} - \mathbf{u}_{ij}$, is determined by two location vectors, it is straightforward to obtain correlation coefficients in the matrix, $\Sigma_{XX}$, from a target correlation model (i.e. eq. 1 and model parameters in Table 2). Note that $\rho(X(\mathbf{u}_{ij}), X(\mathbf{u}_{pq}))$ should have the same value as long as the separation vector, $\mathbf{h} = \mathbf{u}_{pq} - \mathbf{u}_{ij}$, is the same since the correlation is defined as a function of $\mathbf{h}$ as shown in eq. (1):

$$\Sigma_{XY} = \sigma_X \sigma_Y \begin{pmatrix} \rho(X(\mathbf{u}_{11}), Y(\mathbf{u}_{11})) & \rho(X(\mathbf{u}_{11}), Y(\mathbf{u}_{12})) & \dots & \rho(X(\mathbf{u}_{11}), Y(\mathbf{u}_{MN})) \\ \rho(X(\mathbf{u}_{12}), Y(\mathbf{u}_{11})) & \rho(X(\mathbf{u}_{12}), Y(\mathbf{u}_{12})) & \dots & \rho(X(\mathbf{u}_{12}), Y(\mathbf{u}_{MN})) \\ & \dots & & \\ \rho(X(\mathbf{u}_{MN}), Y(\mathbf{u}_{11})) & \rho(X(\mathbf{u}_{MN}), Y(\mathbf{u}_{12})) & \dots & \rho(X(\mathbf{u}_{MN}), Y(\mathbf{u}_{MN})) \end{pmatrix}. \tag{A3}$$

Please note that the diagonal components in the cross-correlation matrix may not be one in certain cases. The correlation maximum can also be placed in the off-diagonal elements in the cross-correlation matrix.

## APPENDIX C

Because $E\{\mathbf{Z}\} = 0$, $E\{\mathbf{X}\} = \mu + \mathbf{L}0 = \mu$. Also, since $\mathrm{Cov}(\mathbf{Z}) = \mathbf{I}$, and $\mathrm{Cov}(\boldsymbol{\mu}) = 0$, $\mathrm{Cov}(\mathbf{X}) = \mathrm{Cov}(\mu + \mathbf{LZ}) = \mathbf{LIL}^T = \boldsymbol{\Sigma}$.

If random vector, $\mathbf{Z}$, follows the multivariate Gaussian distribution, its linear transformation ($\mathbf{X} = \mathbf{LZ} + \mu$) will follow the multivariate Gaussian distribution. We already prove that $E\{\mathbf{X}\} = \mu$ and $\mathrm{Cov}(\mathbf{X}) = \boldsymbol{\Sigma}$, respectively.

You can also see appendix B.5 in Aster *et al*. (2005, pp. 264–265).

## SUPPORTING INFORMATION

Additional Supporting Information may be found in the online version of this article:

**Figure S1.** 1-point statistics of kinematic source parameters extracted from the reverse event in Fig. 3. (a) Marginal probability density function for three-source parameters with stationarity assumption. (b) Depth-dependency of 1-point statistics. The solid and dashed blue lines denote mean and 1-sigma range at the given depth, respectively.
**Figure S2.** Marginal probability density functions (mPDF) obtained for four different depth ranges for the reverse event in Fig. 3.
**Figure S3.** 1-point statistics of kinematic source parameters extracted from the strike-slip event in Fig. 3. (a) Marginal probability density function for three-source parameters with stationarity assumption. (b) Depth-dependency of 1-point statistics. The solid and dashed blue lines denote mean and 1-sigma range at the given depth, respectively.
**Figure S4.** Marginal probability density functions (mPDF) obtained for four different depth ranges for the strike-slip event in Fig. 3.
**Figure S5.** 2-point correlation structure extracted from the reverse event in Fig. 3(b).
**Figure S6.** 2-point correlation structure extracted from the strike-slip event in Fig. 3(c).
**Figure S7.** Pseudo-dynamic source models obtained from stochastic modelling with given 1-point and 2-point statistics for the reverse event in Fig. 3(b). The rest is the same with Fig. 9.
**Figure S8.** Pseudo-dynamic source models obtained from stochastic modelling with given 1-point and 2-point statistics for the strike-slip event in Fig. 3(c). The rest is the same with Fig. 9.
**Figure S9.** Pseudo-dynamic source models after the perturbation of 1-point statistics.
**Figure S10.** Waveforms at five selected stations in Fig. 10 after the perturbation of 1-point statistics.
**Figure S11.** Pseudo-dynamic source models after the perturbation of 2-point statistics.
**Figure S12.** Waveforms at five selected stations in Fig. 10 after the perturbation of 2-point statistics (http://gji.oxfordjournals.org/lookup/suppl/doi:10.1093/gji/ggt479/-/DC1).